Journal of Power Sources 195 (2010) 3720–3729

Contents lists available at ScienceDirect

Journal of Power Sources

journal homepage: www.elsevier.com/locate/jpowsour

Effect of entropy change of lithium intercalation in cathodes and anodes on Li-ion battery thermal management

Vilayanur V. Viswanathan*, Daiwon Choi, Donghai Wang1 [1], Wu Xu, Silas Towne, Ralph E. Williford, Ji-Guang Zhang, Jun Liu, Zhenguo Yang

Pacific Northwest National Laboratory, P.O. Box 999, Richland, WA 99352, USA

ARTICLE INFO

Article history:
Received 21 October 2009
Received in revised form
13 November 2009
Accepted 25 November 2009
Available online 2 December 2009

Keywords:
Lithium-ion
Battery
Entropy
Reversible
Irreversible
Safety

ABSTRACT

The entropy changes (ΔS) in various cathode and anode materials, as well as in complete Li-ion batteries, were measured using an electrochemical thermodynamic measurement system (ETMS). $LiCoO_2$ has a much larger entropy change than electrodes based on $LiNi_xCo_yMn_zO_2$ and $LiFePO_4$, while lithium titanate based anodes have lower entropy change compared to graphite anodes. The reversible heat generation rate was found to be a significant portion of the total heat generation rate. The appropriate combinations of cathode and anode were investigated to minimize reversible heat generation rate across the 0–100% state of charge (SOC) range. In addition to screening for battery electrode materials with low reversible heat, the techniques described in this paper can be a useful engineering tool for battery thermal management in stationary and transportation applications.

1. Introduction

Li-ion batteries are used in a variety of applications requiring charge–discharge rates in the 8-h (*C*/8) to 0.5 h (2C rate) range. While hybrid electric vehicle (HEV) batteries have a high power/energy (P/E) ratio, batteries for plug-in hybrid electric vehicles (PHEVs) are typically discharged over a 4-h period (*C*/4 rate). The power load on HEV/PHEV batteries during acceleration, hill climbing and regenerative braking is quite high, requiring good heat dissipation for peak loads. Electric vehicle batteries are expected to be discharged over an 8-h period (*C*/8 rate). With increasing market penetration of renewables and HEV/PHEVs, the demand for energy storage devices is expected to increase exponentially. These batteries are expected to provide various ancillary services such as voltage regulation, load leveling and load following, with charge–discharge rates ranging from *C*/4 to *C* rates. Unlike typical consumer batteries, these batteries range in size from 4 kWh to 40 kWh, with various P/E ratios. While active cooling is an option for HEV/PHEV/EV batteries, batteries for distributed energy storage at the consumer end are expected to be housed in "transformer boxes", without active cooling. Thermal management becomes more critical, since the surface area/volume ratio of these batteries decreases with increasing battery size, resulting in lower heat transfer rate per unit rate of heat generation [1]. Our previous work has shown that for a single Li-ion polymer cell, there is a temperature increase of 5–20 °C at 1 °C rate, with the temperature increase higher at low SOC [2].

The entropy change ΔS can contribute more than 50% of the total heat generated (in Joules) at the *C*/1 discharge rate [3]. The relative contribution of reversible heat from ΔS is expected to be higher at lower charge–discharge rates. While it is certainly useful to determine the total reversible heat generated during charge or discharge, in certain SOC ranges, the rate of reversible heat generation can be extremely high. Hence it is also important to quantify the rate of reversible heat generation at various SOCs and determine its fraction of total rate of heat generation at each SOC. This can serve as a tool for the battery management system to control battery load or charge current at various SOCs such that high temperature excursions are effectively prevented. While the internal resistance (and hence the irreversible heat generation rate) can be minimized by suitable electrode and cell design, the reversible heat generation rate can play a significant role especially in cases when internal resistance has been minimized.

* Corresponding author at: Pacific Northwest National Laboratory, 902 Battelle Blvd, P.O. Box 999, Richland, WA 99352, USA. Tel.: +1 509 372 4745; fax: +1 509 375 2186.
E-mail address: vilayanur.viswanathan@pnl.gov (V.V. Viswanathan).
[1] Present address: The Pennsylvania State University, 328 Reber Building, University Park, PA 16802, USA.

0378-7753/$ – see front matter © 2009 Elsevier B.V. All rights reserved.
doi:10.1016/j.jpowsour.2009.11.103

Measurement of individual electrode and full cell entropy change, along with computation of reversible and irreversible heat generation rates at various current densities is expected to contribute significantly to effective thermal management for large batteries. Various researchers have determined entropy change values for $LiCoO_2$ [4], $LiCoO_2$ modified with Ni [5], spinel $LiMn_2O_4$ [6], $Li_{1.156}Mn_{1.844}O_4$ [7], $LiFePO_4$ [8], graphite [9], $Li_{4/3}Ti_{5/3}O_4$ spinel [7], and $LiCoO_2$–graphite full cells [1]. From these data, it is apparent that certain cathode/anode couples can be conducive to lower rate of reversible heat generation due to cathode and anode entropy changes canceling out each other at a given SOC across the desired SOC range.

The rate of irreversible heat generation can be determined from impedance measurements for 18,650 cells, with impedance normalized by capacity. Reported impedance values for 18,650 cells [10–13] and prismatic cells [14,15] were compiled, from which normalized values of Ω Ah were calculated.

2. Reversible heat generation rate for lithium-ion batteries

2.1. Entropy change data from the literature

The thermodynamic properties (entropy change, ΔS) of cathode and anode materials were compiled in this work. While data on $LiCoO_2$, spinel $LiMn_2O_4$ cathodes and graphite anode was readily available [4–7,9], only limited information was available on novel electrodes such as $LiFePO_4$ [8] and lithium titanates [7]. The entropy change of the full cell was computed from individual electrode data, while the full cell entropy change for $LiCoO_2$–graphite was obtained from the literature[1]. For some of the literature data, ΔS was calculated from the $\partial E/\partial T$ values [5].

2.2. Reversible and irreversible heat

The reversible heat generation rate [2] Q_r in watts, generated by an electrode is given by

$$Q_r = T\Delta S\frac{I}{nF} \quad (1)$$

where I is the current density (A cm^{-2}), T is temperature (K), ΔS is entropy change (J mole^{-1} K^{-1}), n equals the number of electrons per reaction, and F is the Faraday constant (96,485 C equiv.$^{-1}$). The ETMS instrument ETMS-1000 (Viaspace Inc. Irvine, CA, USA) calculates entropy change based on one Li^+ exchange during charge or discharge, from the equation

$$\Delta S = \frac{nF\partial E}{\partial T} \quad (2)$$

where E is the open circuit potential. Hence, for calculation of rate of reversible heat generation, n is taken to be equal to 1.

The entropy change ΔS typically corresponds to a reduction reaction, which is the discharge reaction for a cathode in a full cell. Depending on convention, the sign for heat generation can be either positive or negative for an exothermic reaction. Assuming heat for an exothermic reaction is negative, discharge current is taken to be positive in sign (and charge current taken as negative) for Eq. (1) to be consistent. (If the heat generation term for exothermic reactions is positive, discharge current has to be negative for consistency.)

It should be noted that during discharge of a Li-ion cell, while reduction takes place at the cathode, oxidation takes place at the anode. Hence, the total change in entropy for a cell during discharge is

$$\Delta S = \Delta S_c + \Delta S_a \quad (3)$$

where ΔS_c corresponds to the entropy change of the cathode material for a reduction reaction, while ΔS_a corresponds to the entropy change of the anode material for an oxidation reaction. Hence the measured or reported ΔS values for anode materials are reversed in sign and presented as ΔS_a in this work in order for Eq. (3) to be consistent.

Since the ETMS instrument does not differentiate between an anode or cathode, the state of charge (SOC) as measured by the instrument increases during oxidation. Since a fully oxidized state for an anode corresponds to 0% SOC in a full cell, the SOC for anode presented in this paper has been adjusted to be equal to the actual SOC for anode in a full cell. Hence, if the instrument SOC for anode is x%, the SOC of the anode, presented in this work, is $(100 - x)$%.

Combinations of cathodes and anodes with low full cell ΔS values were determined across the 0–100% SOC range. In some cases, the low full cell ΔS values were due to low ΔS values of the cathode and anode, while in other cases, the cathode and anode entropy changes were opposite in sign at each SOC, thus minimizing their sum.

The irreversible heat generation rate, Q_{irr} is always exothermic, and is given by

$$Q_{irr} = -I^2R_i \quad (4)$$

where R_i is internal resistance. Eq. (4) states that the irreversible heat generation rate is the product of current I and cell overpotential η_{cell}, with the cell overpotential η_{cell} being the product of cell current I and cell internal resistance R_i, where R_i is the sum of ohmic, activation and diffusion polarization resistances.

The analysis was carried out for a 16 kWh battery (200 V/80 Ah), which is the estimated size for a 40-mile plug-in hybrid electric vehicle (PHEV) battery [16] or estimated size for distributed community energy storage [17]. Using a nominal cell voltage of 3.6 V, the number of cells were calculated, and the total internal resistance of the battery computed from Ω Ah values obtained from the literature [10–15]. The total heat generation rate Q is given by

$$Q = Q_r + Q_{irr} \quad (5)$$

While Q_{irr} is always negative, Q_r can be either positive or negative at various state of charges (SOCs), with the signs being opposite for charge and discharge.

The total heat generation rate was computed for various combination of cathodes and anodes across the 0–100% SOC range. For this work, the internal resistance of the cell was assumed to be the same for all chemistries. As seen later, the internal resistance of the cell is assumed to be at the upper end of the values reported in the literature, and is ~4–5 times that of the lower range of reported internal resistance values. This results in a conservative estimate of the contribution of reversible heat generation rate, since for cells with lower internal resistance, the contribution from reversible heat generation would be higher as a percentage of total heat generation rate.

In a typical $LiCoO_2$/C battery, the overall electrochemical reaction for discharge can be expressed as:

$$2Li_{1-x}CoO_2 + Li_{2x}C_6 \leftrightarrow 2Li_{1-x+y}CoO_2 + Li_{2x-2y}C_6 \quad (6)$$

where $x < 0.5$ and $y < x$.

The corresponding entropy change in this battery for the reaction is the sum of the individual electrode entropy change, as written, is:

$$\Delta S_{cell} = \Delta S_{Li_{1-x+y}CoO_2} + \Delta S_{Li_{2x-2y}C_6} \quad (7)$$

[2] Please note that all references to heat in this work correspond to heat generation rate in watts.

Table 1
List of electrodes and full cells.

Chemistry	Label	Literature reference/source
Cathodes		
$LiCoO_2$	LCO-LICO	Procured from LICO Corp.
$LiCoO_2$	LCO-A	Procured from manufacturer A
$LiCoO_2$	LCO-L	Reynier et al. [4]
$LiNi_{0.7}Co_{0.3}O_2$	$LiNi_{0.7}Co_{0.3}O_2$-L	Funahashi et al. [5]
$LiNi_xCo_yMn_zO_2$	$LiNi_xCo_yMn_zO_2$-LiCO	Procured from LICO Corp.
$LiFePO_4$	LFP-NEI	Obtained from NEI Corp.
$LiFePO_4$	LFP-PNNL	Synthesized at PNNL
$LiFePO_4$	LFP-L	Yamada et al. [8]
$LiMn_2O_4$	LMO-L	Yazami et al. [6]
$Li_{1.156}Mn_{1.844}O_4$	$Li_{1.156}Mn_{1.844}O_4$-L	Lu et al. [7]
Anodes		
Graphite	G-L	Reynier et al. [9]
Graphite	G-A	Procured from manufacturer A
Anatase TiO_2/graphene	Anatase TiO_2-PNNL	Synthesized at PNNL
$Li_{4/3}Ti_{5/3}O_4$	LTO-L	Lu et al. [7]
Li titanate	LTO-NEI	Procured from NEI Corp.
Full cell		
$LiCoO_2$–graphite	FC LCO/G-L	Onda et al. [1]. FC: full cell
$LiFePO_4$–titanate	FC LFP/LTO-NEI	Procured from NEI Corp. FC: full cell

The rate of reversible heat generation from the $LiCoO_2$ cathode and the graphite anode at each SOC can be calculated from Eq. (1). In this study, since various cathodes and anodes have been studied, the entropy change and heat generation rate is plotted as a function of SOC, since the x values can vary depending on cathode or anode. Also, the sign of entropy change for the anode is reversed from the reported or measured data, since the reported or measured values correspond to reduction reactions for all electrodes, while, as discussed earlier, oxidation occurs at the anode during discharge.

3. Experiment

3.1. Electrode synthesis

Nanosized $LiFePO_4$ was synthesized using $LiCoOCH_3{\bullet}2H_2O$ (reagent grade, Sigma), $FeCO_2{\bullet}2H_2O$ (99%, Aldrich), $(NH_4)H_2PO_4$ (99.999%, Sigma–Aldrich), oleic acid (FCC, FG) and paraffin wax (ASTM D 87, mp. 53–57 °C, Aldrich). $(NH_4)H_2PO_4$ was ball-milled with oleic acid for 1 h using high energy mechanical mill (HEMM, SPEX 8000M) in a stainless steel vial. After paraffin wax was added and milled for 30 min, iron oxalate was added and milled for 10 min. Finally, Li acetate was added and milled for 10 min. The overall molar ratio was Li:Fe:P:oleic acid:paraffin = 1:1:1:1:2. The precursor paste was dried in an oven at 110 °C for 30 min followed by heat-treatment in a tube furnace at 500 °C for 8 h under UHP-3%H_2/97%Ar gas flow with a temperature ramp rate of 5 °C min^{-1}. After the $LiFePO_4$ was obtained, 10 wt% carbon black was milled in a planetary mill for 4 h (Retsch 100CM) at 400 rpm. TiO_2/graphene composite (2.5 wt% graphene) was obtained by a self-assembly approach following our previous work [18]. Microstructures were analyzed by field emission scanning electron microscopy (FE-SEM) (FEI Nova 600) and high resolution transmission electron microscopy (HRTEM).

3.2. Entropy measurement

Entropy data of cathodes, anodes, and complete cells were obtained by monitoring the change in open circuit voltage as a function of temperature using ETMS-1000. Several cathode and anode powders were obtained from LICO Technology Corp. Cathodes and anodes were prepared by mixing 85% active material, 10% poly (vinylidene fluoride) (PVDF) binder (Alfa Aesar), and 5% carbon black (Super P-Li, Timcal) in N-methylpyrrolidone (NMP) (Aldrich), and then cast on Al and Cu foils, respectively. Customer-coated cathode and anode films obtained from Manufacturer A were used as received for entropy measurement. To measure entropy changes in cathodes or anodes, they were assembled in a Type-2325 coin cell in an argon-filled glove box with a 0.75 mm-thick, Li-foil anode (Aldrich) and microporous polypropylene separator (Celgard 2501). The electrolyte used was 1 M $LiPF_6$ in a 1:1 mixture of ethylene carbonate (EC) and dimethyl carbonate (DMC) (EM Industries), using a coin cell crimper (National Research Council, Canada). Complete cells with various cathodes and anodes also were assembled using a similar procedure to that described above by replacing Li metal with the appropriate anode.

The $LiFePO_4$ cathode cells were cycled at $C/10$ rate between 2.5 V and 4.1 V. The voltage range for TiO_2 anode cells was 1–3 V. After three cycles, the cells were brought to a fully discharged state prior to the start of entropy determination. Charge stabilization was done at 35 °C for 2 h, followed by returning the cell temperature to the initial desired value. The initial temperature was set to be equal to the charge stabilization temperature. After 15 min at this initial temperature, the cell voltage was measured, and then the cell temperature was changed to the next value (e.g., 25 °C). After temperature equalization at that temperature, the cell voltage was measured at the end of the period, and then the temperature was changed to the next level (e.g., 15 °C). The cell temperature was then brought to the initial value (35 °C) to determine drift from the initial voltage reading. Entropy changes were calculated from the slope of the voltage–time curve using Eq. (2). The ETMS software has an auto-correct feature that adjusts for drift in cell open circuit voltage due to self-discharge by adjusting the slope of voltage vs. temperature to account for the self-discharge.

It should be note that the ΔS values include entropy change for the reference Li/Li^+ electrode. Since reported values in the literature for other half cells are also against the same reference, various cathode and anode combinations can be simulated, since the contribution from the Li/Li^+ reference electrode will cancel out. Moreover, since the reference electrode is lithium metal, there is negligible change in the electrode entropy as lithium is added to or subtracted from that electrode during charge or discharge.

The experiments were repeated for $LiFePO_4/TiO_2$ cells, using voltage limits of 0.25 V and 3 V. While ΔH and ΔS values were computed by the ETMS software from the voltage vs. temperature data, only ΔS values are reported in this work, since only these values are relevant to reversible heat generation.

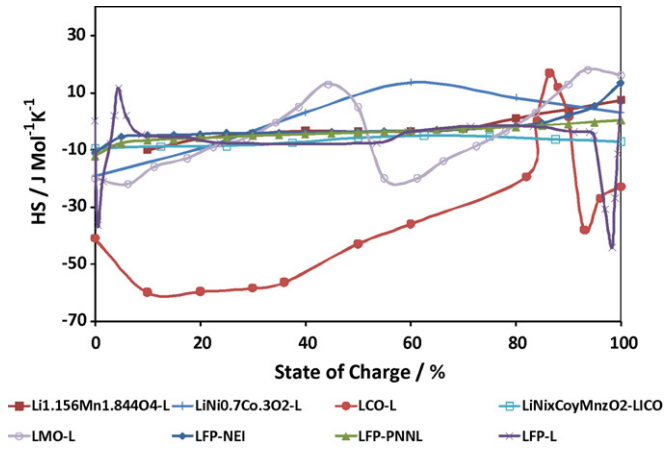

Fig. 1. Comparison of entropy change ΔS for various cathodes. L: literature data, PNNL: synthesized and tested at PNNL, LiCo and NEI procured from LICO Corp. & NEI Corp. and tested at PNNL.

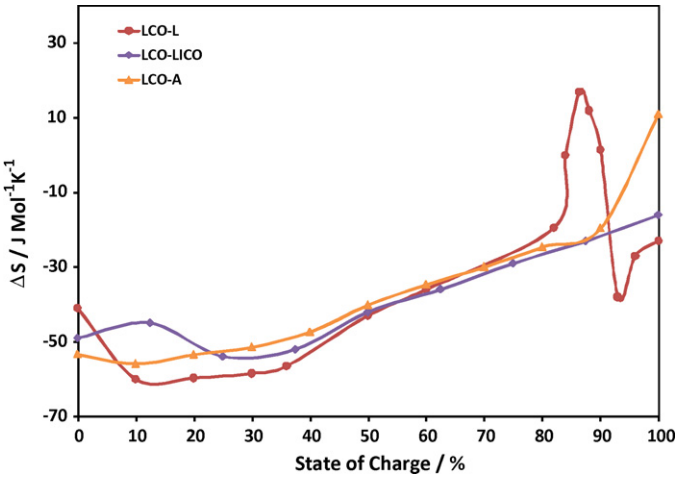

Fig. 3. Comparison of entropy change ΔS for $LiCoO_2$ cathodes.

4. Experimental and simulation results

The entropies of the cathodes and anodes were obtained from the literature. Some measurements for $LiCoO_2$ and modified $LiCoO_2$, such as $LiNi_xCo_yMn_zO_2$, obtained from LICO Corp., and $LiCoO_2$ obtained from Manufacturer A were conducted using the ETMS. Commercial $LiFePO_4$ and lithium titanate (LTO) from NEI Corp. along with $LiFePO_4$ cathode and anatase TiO_2–graphene anode synthesized at PNNL were also tested in the ETMS. Fully assembled cells of $LiFePO_4$ and LTO from NEI Corp. were also tested. A list of electrodes and fully assembled cells referred to in this work are given in Table 1.

Fig. 1 shows the ΔS entropy for all cathodes, while Fig. 2 shows ΔS for all anodes. The ΔS values for $LiCoO_2$ was significantly higher than other cathodes, while modification with Ni and Mn resulted in much lower ΔS for $LiNi_xCo_yMn_zO_2$. However, $LiCoO_2$ modification without Mn presence showed higher ΔS values as seen for $LiNi_{0.7}Co_{0.3}O_2$. $LiMn_2O_4$ and its modification such as $Li_{1.156}Mn_{1.844}O_4$ have low ΔS, while $LiFePO_4$ procured from NEI Corp. and synthesized at PNNL, along with the literature reported value (LFP-L), have extremely low ΔS values across 0–95% SOC. Among anodes, graphite has higher ΔS values, while the $Li_{4/3}Ti_{5/3}O_4$ lithium titanates (LTOs) as reported in the literature and the LTO procured from NEI Corp. had very low ΔS. The anatase TiO_2–graphene synthesized at PNNL had higher ΔS value compared to lithium titanates.

Fig. 3 compares the entropy change for $LiCoO_2$ from the literature with results for the sample procured from LICO Corp. & Manufacturer A, as measured at PNNL. The agreement is reasonably good, with slight differences among various manufacturers/sources. Fig. 4 compares the graphite entropy change from the literature with results for the sample procured from Manufacturer A and measured at PNNL. Again, the literature value agrees well with PNNL measured values.

For the anodes, in this work, the ΔS values have been presented for the oxidation reaction. This is opposite in sign to measured or reported values, since ΔS values are typically reported for the reduction reaction. Also, the ETMS assumes 0% SOC for the reduced state, while the reduced state corresponds to 100% SOC for anodes in a full cell. Hence the anode ΔS presented in this work corresponds to the discharge reaction for the anode, and the anode SOC values refer to actual anode SOC in a full cell. While $LiFePO_4$ and lithium titanates (LTOs) have the lowest ΔS values, mixing and matching other cathode–anode pairs provided ΔS values for full cells, that are competitive with those of $LiFePO_4$/LTO full cells. This was due to the complementary effects of the electrodes, such that entropy values for each electrode were approximately equal in magnitude while being opposite in sign to each other at a fixed SOC in the 0–100% SOC range. Fig. 5 shows some promising cath-

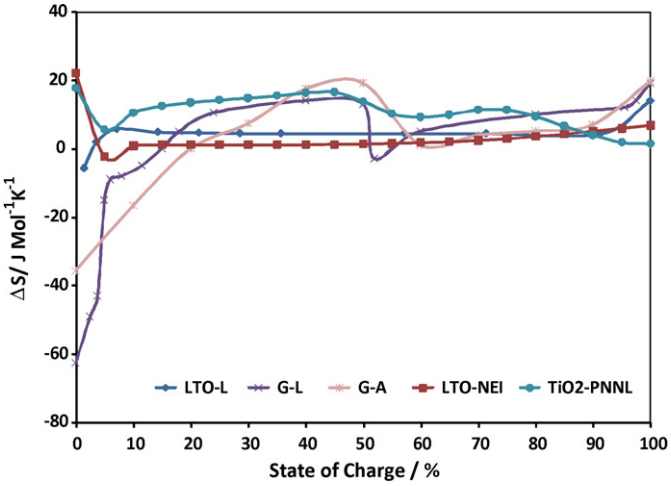

Fig. 2. Comparison of entropy change ΔS for various cathodes.

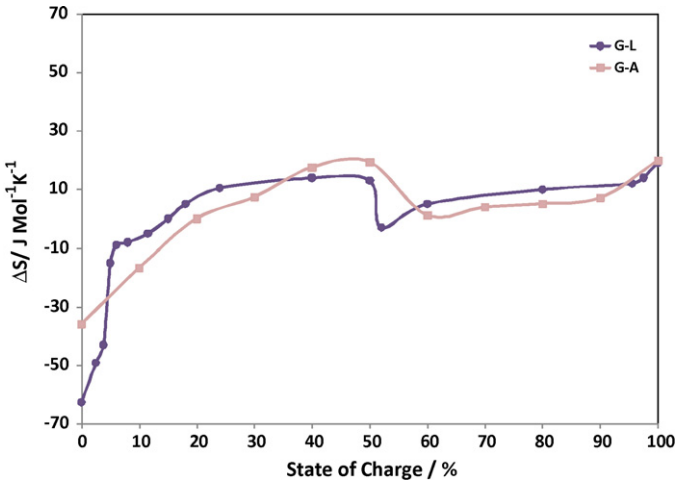

Fig. 4. Comparison of entropy change ΔS for graphite anodes.

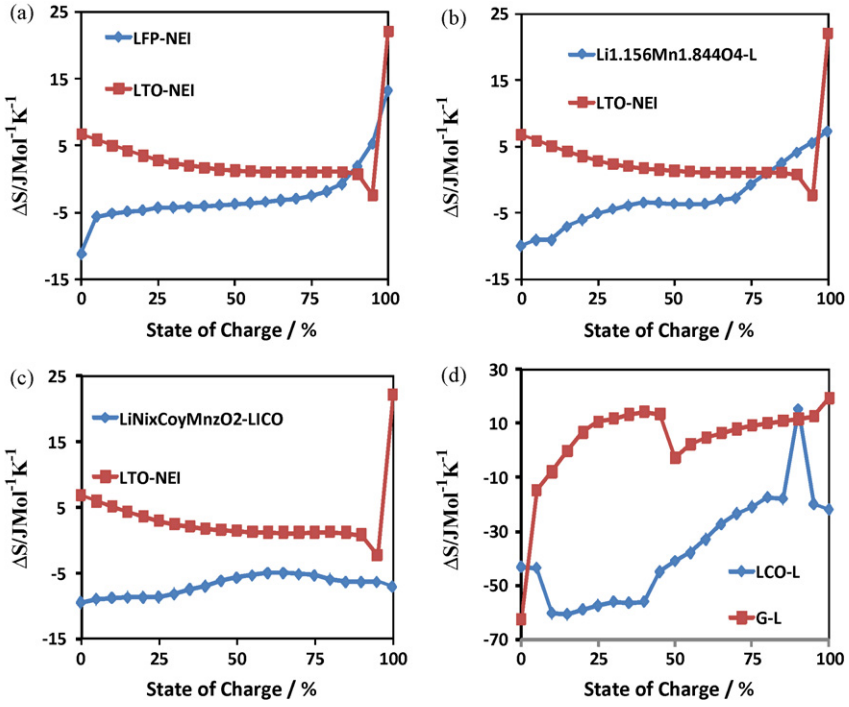

Fig. 5. Complementary effect of anode and cathode entropy change ΔS for various cathode–anode combinations.

ode/anode combinations that have such a complementary effect. Among electrodes that have low ΔS values, $LiFeOP_4$–LTO (Fig. 5a), $Li_{1.156}Mn_{1.844}O_4$–LTO (Fig. 5b) and $LiNi_xCo_yMn_zO_2$–LTO (Fig. 5c) have cathode and anode entropies that are opposite in sign at a fixed SOC across the 0–100% SOC range. For $LiCoO_2$–graphite, where both cathode and anode ΔS values are high, the opposing signs of cathode and anode ΔS has a slight beneficial effect (Fig. 5d).

Full cell entropies calculated for various electrode combinations are shown in Fig. 6. As expected, $LiCoO_2$ based cells have a high change in entropy, while full cell ΔS values were low in magnitude for the following combinations:

- $LiFePO_4$/LTO
- $LiFePO_4$–graphite
- $LiNi_xMn_xCo_xO_2$/LTO
- $Li_{1.156}Mn_{1.844}O_4$/LTO
- $LiNi_xMn_xCo_xO_2$/graphite
- $Li_{1.156}Mn_{1.844}O_4$/LTO

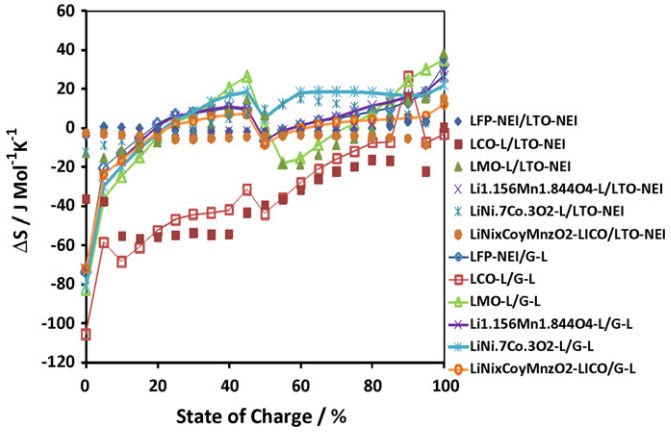

Fig. 6. Computed full cell ΔS from individual electrode ΔS.

Fig. 7 shows the average ΔS values for all electrodes, with ΔS being the average of absolute ΔS values across the 0–100% SOC range. This figure provides a snapshot of ΔS values for all leading cathode–anode combinations, and can serve as a screening tool for various cathode and anode combinations. $LiCoO_2$ based cathodes with both graphite and LTO anodes have high ΔS values, while values for $LiFePO_4$ cathodes have very low entropy change, especially in combination with LTO anodes. Modification of $LiCoO_2$ with nickel and manganese ($LiNi_xMn_xCo_xO_2$), and non-stoichiometric $LiMn_2O_4$ ($Li_{1.156}Mn_{1.844}O_4$) decreased the ΔS for the cell, especially in combination with LTO anode. While most of the data in this figure are calculated from individual electrode val-

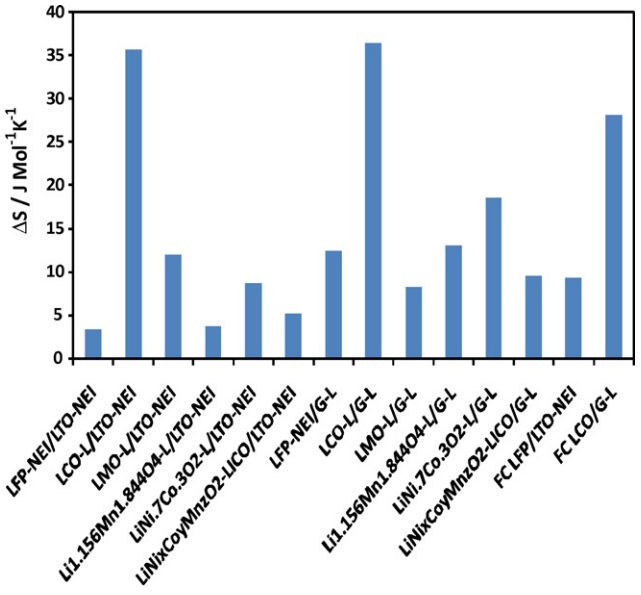

Fig. 7. Average of absolute value of computed full cell entropy change over the 0–100% SOC range. FC LFP/LTO-NEI and FC LCO/G-L (last 2 columns) correspond to average of measured entropy change for full cells.

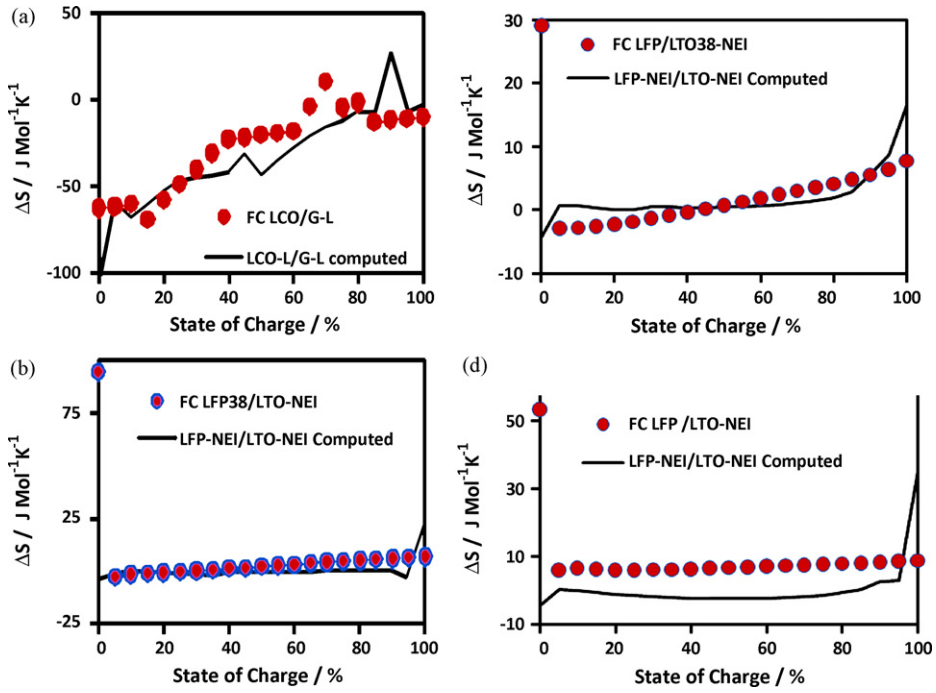

Fig. 8. Comparison of full cell and computed values of ΔS. (a) $LiCoO_2$/graphite; (b and c) $LiFePO_4$/Li titanate; (b) 38% excess $LiFePO_4$; (c) stoichiometric and (d) 38% excess Li titanate.

ues, the last two samples correspond to full cell values, with FC LFP/LTO-NEI measured at PNNL for the $LiFePO_4$–LTO full cell, while the FC LCO/G-L was reported values for $LiCoO_2$–graphite full cell [1].

While most full cell ΔS values reported in this work have been calculated from individual electrode values from the literature and/or measured at PNNL, some limited full cell measurements were conducted at PNNL on $LiFePO_4$–titanate cells with stoichiometric electrode composition, 38% $LiFePO_4$ excess and 38% lithium titanate excess. Reported full cell ΔS values for $LiCoO_2$–graphite were also used to compare results with computed values from individual electrode data. Fig. 8a shows the results for $LiCoO_2$–graphite, while Fig. 8b–d shows results for LFP–LTO with cathode excess, anode excess and both electrodes in stoichiometric amounts respectively. For cells with excess $LiFePO_4$ and excess LTO, the SOC for the electrode in excess was assumed to vary from 0 to 62% in order to calculate full cell entropy from individual cell data. The agreement between reported/measured full cell values and computed values was good.

Based on these results, various electrode combinations were selected for calculation of reversible and total heat generation rate during charge and discharge. For this work, it was assumed that irreversible heat was the same for all cell chemistries and SOCs. The internal resistance of various Li-ion cells was obtained from the literature and summarized in Table 2. The internal resistance, as discussed earlier, included ohmic, activation and diffusion polarization resistances. The internal resistance values were multiplied by the capacity of the cell to get capacity normalized resistance values. The capacity normalized values were about the same for the 18,650 and prismatic cells with various cathodes. While most cells had a normalized impedance of 0.16–0.23 Ω Ah, some high power cells had impedance of 0.04–0.06 Ω Ah. The cells with high impedance had $LiCoO_2$ based cathodes, while cells with ~0.16–0.19 Ω Ah correspond to layered cathodes containing various combinations of

Table 2
AH-normalized internal resistance (IR) of Li-ion cells.

IR (ohms)	Capacity (Ah)	Normalized IR (Ω Ah)	Method	Cathode	Source	Notes
0.1	2	0.2	Current interrupt	Doped $LiNiO_2$	[13]	6A pulse discharge (5 s on 25 off) 18,650 cells
0.114	1.4	0.16	Current interrupt	$LiCoO_2$	[10]	18,650 cells provided by Argonne National Laboratory
0.182	0.9	0.164	a.c. Impedance	$LiNi_{.8}Co_{.15}Al_{.05}O_2$	[11]	Electrodes from Quallion, cell fabricated at Sandia 18,650 cells
0.21	1.1	0.23	Current interrupt	$LiCoO_2$	[3]	18,650 cells measured at 35 °C
0.08	2.2	0.176	Not provided	Not provided	Tenergy Corp. data sheet	18,650 cell-resistance includes PTC
0.04	1.3	0.05	a.c. Impedance	$Li(Ni_{1/3}Co_{1/3}Mn_{1/3})$	[12]	High power 18,650 cells
0.025	10	0.23	a.c. Impedance	$LiCoO_2$	[14]	Prismatic cell
0.018	8.3	0.149	Not provided	Not provided	[15][a]	Enax cell
0.022	6.8	0.150	Not provided	Not provided	[15]	Saft LV41-6S battery
0.0046	40	0.184	Not provided	Not provided	[15]	Worley 100216216HP
0.0027	70	0.189	Not provided	Not provided	[15]	Worley 60460330HP
0.016	10	0.160	Not provided	Not provided	[15]	Valence U1-12XP

[a] Impedance data for individual cells from various manufacturers for conversion of Prius to Prius + PHEV.

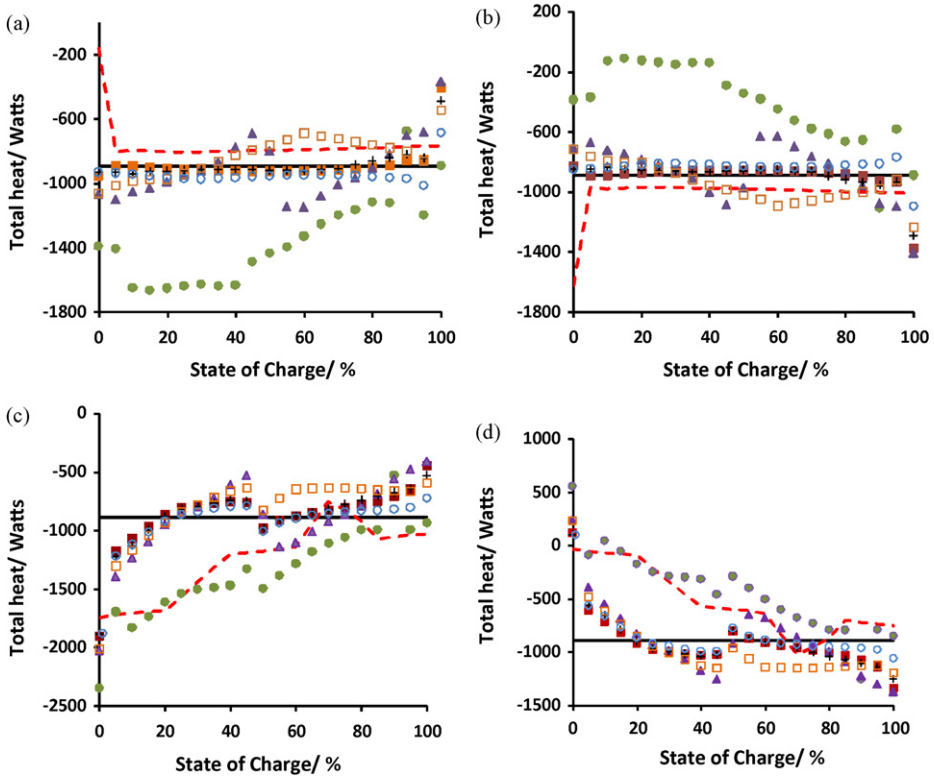

Fig. 9. Sum of irreversible and reversible heat generation rates for *C* rate charge–discharge. (a and b) Li titanate (LTO-NEI) based anodes; (a) discharge; (b) charge; (c and d) graphite (G-L) based anodes; (c) discharge; (d) charge. ▬ Irreversible heat, LFP-NEI, ● LCO-L, ▲ LMO-L, +$Li_{1.156}Mn_{1.844}O_4$-L, □ $LiNi_{.7}Co_{.3}O_2$-L, ○ $LiNi_xCo_yMn_zO_2$-LICO, FC (LFP/LTO-NEI for LTO anodes and LCO/G-L for graphite based anodes).

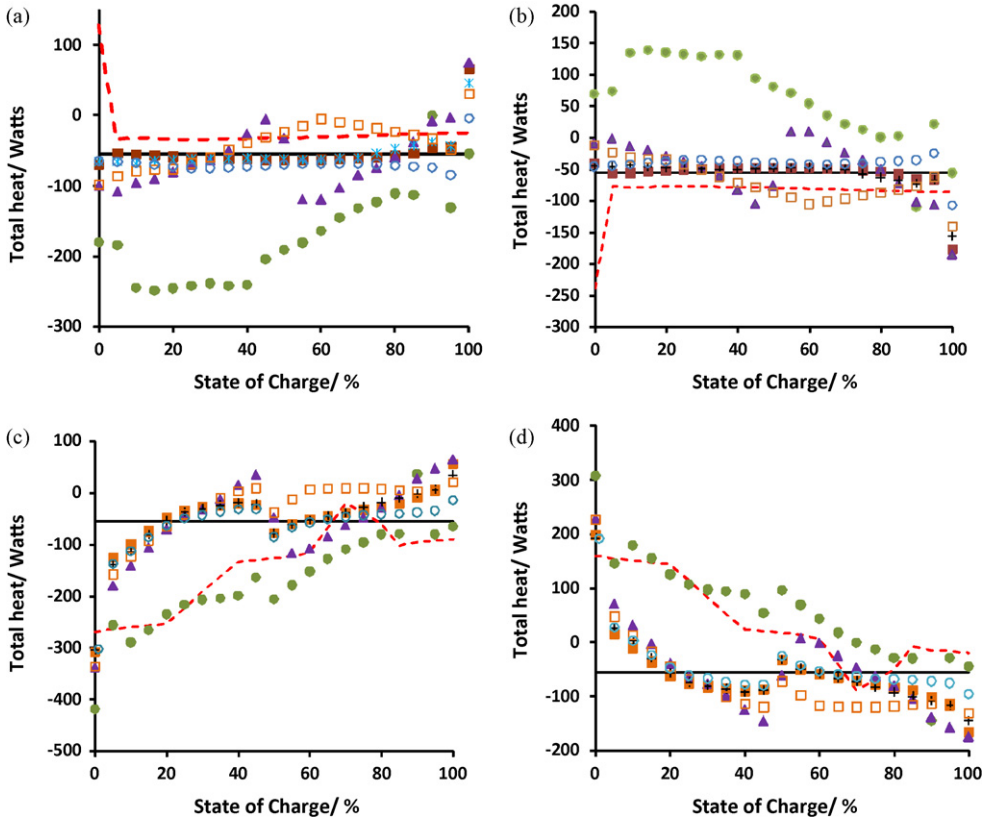

Fig. 10. Sum of irreversible and reversible heat generation rates for *C*/4 rate charge–discharge. (a and b) Li titanate (LTO-NEI) based anodes; (a) discharge; (b) charge; (c and d) graphite (G-L) based anodes; (c) discharge; (d) charge. ▬ Irreversible heat, LFP-NEI, ● LCO-L, ▲ LMO-L, +$Li_{1.156}Mn_{1.844}O_4$-L, □ $LiNi_{.7}Co_{.3}O_2$-L, ○ $LiNi_xCo_yMn_zO_2$-LICO, FC (LFP/LTO-NEI for LTO anodes and LCO/G-L for graphite based anodes).

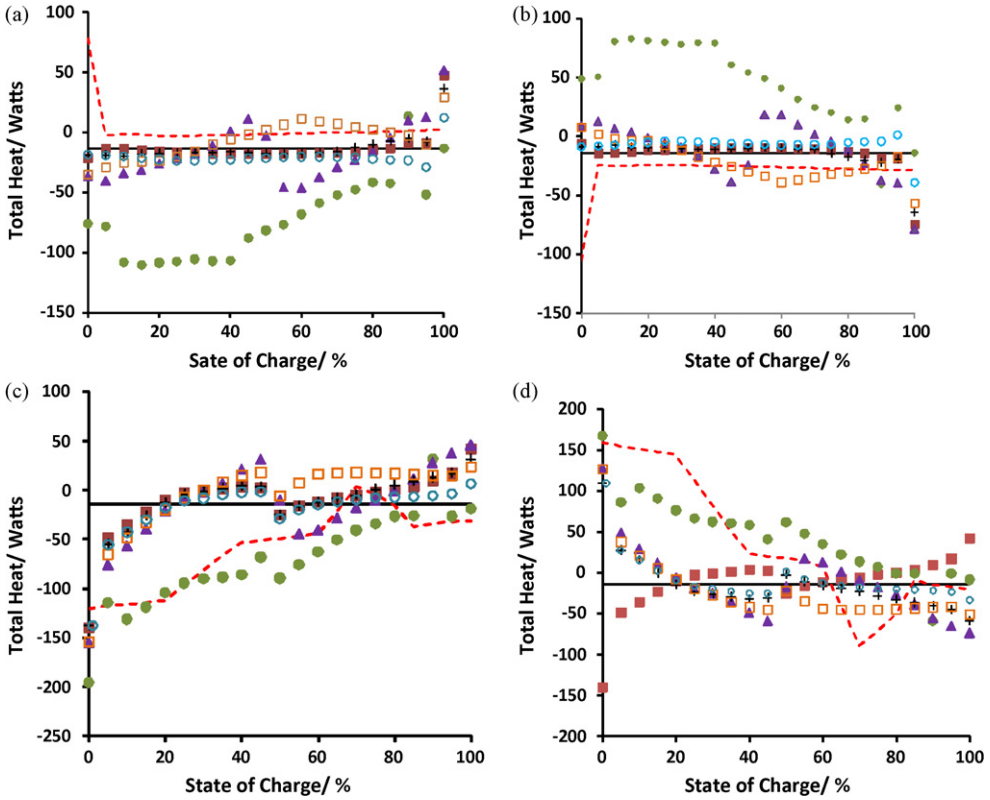

Fig. 11. Sum of irreversible and reversible heat generation rates for *C*/8 rate charge–discharge. (a and b) Li titanate (LTO-NEI) based anodes; (a) discharge; (b) charge; (c and d) graphite (G-L) based anodes; (c) discharge; (d) charge. ▬ Irreversible heat, LFP-NEI, ● LCO-L, ▲ LMO-L, +$Li_{1.156}Mn_{1.844}O_4$-L, □ $LiNi_{.7}Co_{.3}O_2$-L, ○ $LiNi_xCo_yMn_zO_2$-LICO, FC (LFP/LTO-NEI for LTO anodes and LCO/G-L for graphite based anodes).

nickel, cobalt and aluminum. Hence a normalized value of 0.2 Ω Ah, which includes resistance for interconnections, was used in this analysis. For spinel based high rate cells, the normalized impedance is expected to be 3–5 times lower than the value used in this work. Hence for those cells, the contribution from reversible heat generation rate is expected to be 3–5 times higher that the values calculated in this work.

The average power consumption per home for the year 2007 was ~1.3 kW [19]. Assuming distributed community energy storage will require one battery for three homes [16], this corresponds to 3.6 kW, with a total battery energy requirement of 14–15 kWh for 4-h storage. For a 40-mile PHEV, the required battery size is 12 kWh. Since PHEV batteries can also be used to provide load leveling services, the battery size chosen in this study for thermal analysis was 16 kWh (200 V/80 Ah). The internal resistance of each cell was calculated to be 0.0025 Ω (0.2 Ω Ah/80 Ah). Using a nominal cell voltage of 3.6 V $cell^{-1}$, the impedance of a 200 V battery was calculated to be 0.14 Ω. The irreversible heat generation rate at each charge/discharge rate was then calculated from Eq. (4), and was found to be −890 W, −56 W and −14 W at the *C*, *C*/4 and *C*/8 rates respectively.

It has been reported that total reversible heat generated from electrodes can be as high as 50% of the irreversible heat [3]. In order to determine the relative effect of reversible heat on thermal management, Figs. 9–11 show the total heat generation rate for full cells with LTO and graphite based anodes during charge and discharge at various rates. Fig. 9 shows results for *C* rate, while Figs. 10 and 11 show results for *C*/4 and *C*/8 rates respectively. The total rate of heat generation during discharge is calculated from Eq. (5) by adding the irreversible heat (negative sign) and the reversible heat generation rates corresponding to ΔS values for the full cell, where Eq. (3) was used to calculate ΔS for the full cell from individual electrode data. For charge, the total heat generation rate is obtained by adding the irreversible heat to the reversible heat generation rate for charge, which is opposite in sign to that for discharge. In each of these figures, the irreversible heat generation rate has been plotted as a solid line, in order to indicate the range of deviation of total heat generation rate from irreversible heat generation rate across the 0–100% SOC range.

For $LiCoO_2$ based cathodes during charge, there is a cooling effect, with total heat generation rate at *C* rate as low as −150 W for TiO_2 based anodes in the 10–40% SOC range (Fig. 9b), while during discharge, the total heat generation rate is as high as 1500–2200 W in the 5–40% SOC range (Fig. 9a), with the irreversible heat calculated from the literature Ω Ah values equal to −890 W. Such a wide variation in total heat generation rate during charge–discharge leads to significant challenges for battery thermal management for multi-cell batteries. On the other hand, for $LiFePO_4$ based cathodes, the variation in total heat generation rate is very small (10–20 W), especially for titanate based anodes in the 5–95% SOC range. At 100% SOC, the total heat generation rate during charge increases to −1400 W for $LiFePO_4$–titanate cells (Fig. 9b). For $LiFePO_4$–graphite cells, the heat generation rate was 1200–1800 W during discharge in the 0–5% SOC range (Fig. 9c), while it was 1200–1300 W in the 95–100% SOC range during charge (Fig. 9d). Hence, cycling in the 5–95% appears to be highly beneficial for good thermal management in $LiFePO_4$ based cells with either titanate or graphite anodes. While best results were obtained for $LiFePO_4$–titanate full cells, low reversible heat generation rate (and hence low total heat generation rate) was also obtained for Ni–Mn modified $LiCoO_2$ electrodes, and modified spinel $Li_{1.56}Mn_{1.844}O_4$ based cathodes at *C* rate.

Similar results were obtained at *C*/4 (Fig. 10) and *C*/8 (Fig. 11) rates, with the reversible heat generation rate being a higher percentage of irreversible heat generation rate as the charge–discharge rate is decreased. The irreversible heat generation rate at *C*/4 rate was −56 W, while for $LiCoO_2$ cathodes, the total rate of heat genera-

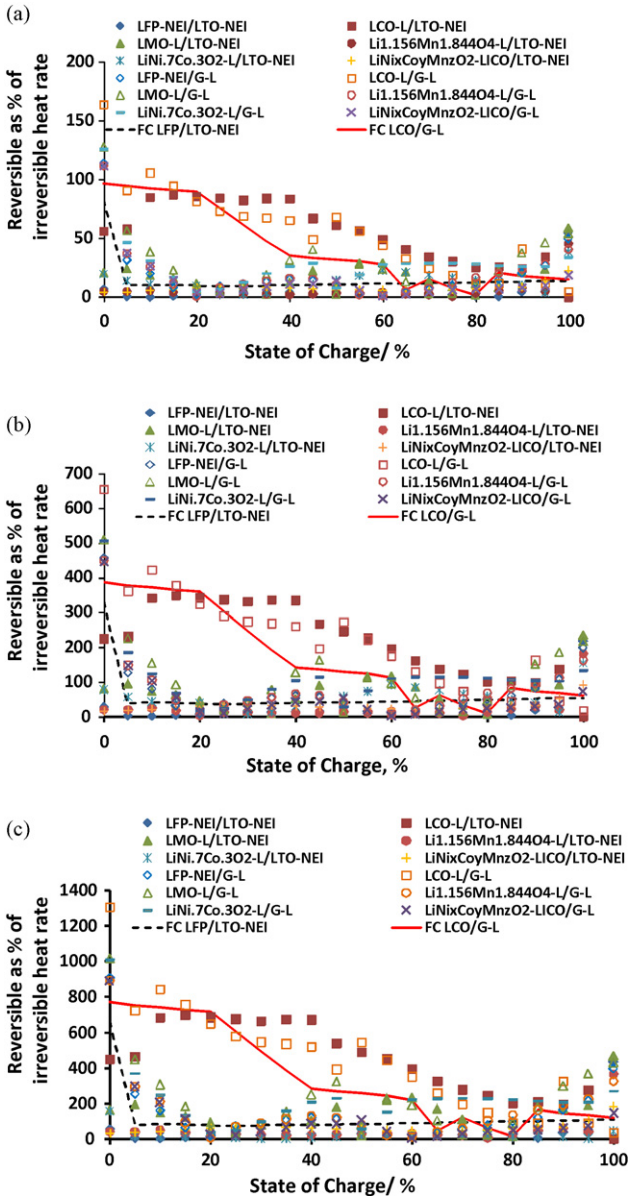

Fig. 12. Contribution of reversible heat generation rate as % of irreversible heat generation rate in the 0–100% SOC range at various rates (a) *C*, (b) *C*/4 and (c) *C*/8.

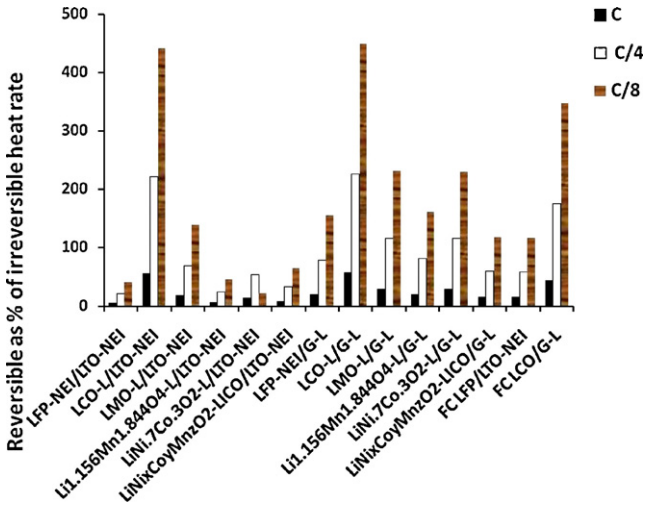

Fig. 13. Contribution of reversible heat generation rate as % of irreversible heat generation rate at various rates—values at each rate averaged over the 0–100% SOC range.

tion was as high as −300 W during discharge in the 0–30% SOC range (Fig. 10a and c), with a net cooling effect of 140 W during charge in the same SOC range (Fig. 10b and d). At *C*/8 rate, the irreversible heating effect was −14 W, while the total rate of heat generation during discharge for cells with $LiCoO_2$ cathodes was −100 W in the 0–40% SOC range (Fig. 11a and c) with a net cooling effect of 80 W during charge (Fig. 11b and d). $LiFePO_4$–titanate full cells, Ni–Mn modified $LiCoO_2$ electrodes, and modified spinel $Li_{1.56}Mn_{1.844}O_4$ based cathodes showed a very low reversible contribution to total heat generation rate at all charge–discharge rates.

For all charge–discharge rates, $LiCoO_2$ based cathodes have a very high reversible contribution to the total heat generation rate. In the 0–40% SOC range, the reversible heat generation rate for $LiCoO_2$ based cathodes was ~5–7*x* irreversible heat generation rate at *C*/8 rate in the 5–40% SOC range, while it was ~0.8*x* of irreversible heat generation rate at *C* rate.

Fig. 12a–c shows the reversible heat generation rate as a percentage of irreversible heat generation rate at *C*, *C*/4 and *C*/8 rates respectively. At 1C rate, the reversible heat generation rate is about 5% for LFP-TiO_2 cells, and around 5–20% for nickel and manganese $LiCoO_2$ and spinel $LiMn_2O_4$ along with its modified form in the 5–95% SOC range (Fig. 12a). However, for $LiCoO_2$ based cathodes, in the 5–40% SOC range, the reversible heat is as high as 80% of irreversible heat, or ~700 W. For the same SOC range, at *C*/4 rate, $LiCoO_2$ based cathodes have a reversible heat generation rate equal to 350% of the irreversible heat, or ~250 W, while the $LiFePO_4$ based and Ni–Mn modified $LiCoO_2$ cathodes have a net contribution of 10–40% for reversible heat in the 5–95% SOC range, with $LiFePO_4$ based cathodes andTiO_2 based anodes having lower heat generation rates (Fig. 12b). At *C*/8 rate, the heat generation rate for $LiCoO_2$ bases cathodes is 700% of the irreversible heat generation rate, or 112 W in the 5–40% SOC (Fig. 12c). Again, the $LiFePO_4$ based and Ni–Mn modified $LiCoO_2$ based cells have a much lower reversible heat generation rate contribution of ~15–60%, with $LiFePO_4$–LTO based cells at the lower end of this range.

Fig. 13 shows the average across all SOC of rate of reversible heat generation as a percent of irreversible heat. Sample labels starting with FC (full cell) correspond to full cell values (measured for LFP/LTO and obtained from the literature for LCO/G as seen in Table 1). The rest of the values are computed from individual electrode values as indicated in Table 1. While the $LiFePO_4$–LTO combination corresponds to lowest reversible heat generation rate contribution, LTO based cells correspond to lower reversible heat generation rates compared to graphite based cells. The importance of cathode and anode selection is clearly evident from this figure.

For utility based applications, the storage requirements are 3–4 h [16]. This is expected to rise to as high as 8 h storage as renewables market penetration increases. Hence the contribution of reversible heat generation is considered to be a key design parameter across the *C*/8–C rate of charge–discharge. This is especially true for distributed energy storage, where active cooling using fans is not an option. The batteries will be designed to fit in a box which may not be extremely conducive to thermal management. For PHEV, the charge–discharge rate is expected to be in the *C*/4–C rate. While thermal management options such as active cooling is expected to be available, the significant differences in reversible heat generation rates among various cathode–anode combinations (as high as 1.5 kW) at *C* rate and 0.7 kW at *C*/4 rate indicate that cathode and anode selection to minimize reversible heat generation rate is crucial for thermal management, affecting safety, performance and battery life. The results of this work can be implemented as a tool in battery management systems (BMS),

with the BMS able to estimate total heat generation rate in the battery at a fixed SOC based on the direction of current flow. The BMS can then pro-actively limit charge–discharge currents to prevent a temperature excursion beyond a preset value, rather than react to the temperature rise after the event.

5. Conclusions

A comprehensive database of entropy for various cathodes and anodes was generated. The entropies changes for various cathode and anode materials, as well as complete Li-ion cells, were investigated using the ETMS. $LiCoO_2$ has a much larger entropy change compared to other cathodes investigated. Graphite has higher entropy change compared to lithium titanate anodes. Some electrode combinations have good synergy, with the entropy of the cathode and anode being mirror images of each other, thus canceling each other out. The reversible heat generation rate comprises ~700% of irreversible heat for $LiCoO_2$ based cells at *C*/8 rate in the 5–40% SOC range, while the contribution from $LiFePO_4$–LTO cells is ~30% of irreversible heat. At *C* rates, the high reversible heat contribution from $LiCoO_2$ based cathodes leads to a wide swing in heat generation rate of 1.4 kW between discharge and charge at a fixed SOC in the 5–40% SOC range, compared to a swing of ~50 W for in the 5–95% SOC range for $LiFePO_4$–LTO cells. Hence, a suitable choice of cathode and anode is expected to mitigate thermal management issues for HEV/PH EV/EV and utility based applications. The results of this analysis will enable prediction of battery temperature excursions during charge/discharge, thus providing a pro-active battery management tool.

Acknowledgments

The research described in this paper was conducted under the Laboratory Directed Research and Development Program at Pacific Northwest National Laboratory, a multi-program national laboratory operated by Battelle for the U.S. Department of Energy. We are also grateful to Dr. Imre Gyuk of the DOE-OE Electricity Storage Program for funding to continue this work, and for helpful discussions with Mr. Tien Duong of the DOE. We sincerely appreciate the significant help provided on the ETMS system by Dr. Joseph C. McMenamin, currently at CFX Battery in Azusa, CA. We are grateful to Dr. Jinxiang Dai and Dr. Ganesh Skandan of NEI Corporation for providing us with $LiFePO_4$ and Li titanate samples.

References

[1] K. Onda, T. Oshima, M. Nakayama, K. Fukuda, T. Araki, J. Power Sources 158 (2006) 535–542.
[2] R.E. Williford, V.V. Viswanathan, J.-G. Zhang, J. Power Sources 189 (2009) 101–107.
[3] J.-S. Hong, H. Maleki, S. Al Hajjaj, L. Redey, J.R. Selman, J. Electrochem. Soc. 145 (5) (1998) 1489–1501.
[4] Y. Reynier, J. Graetz, T.S. Wood, P. Rez, R. Yazami, B. Fultz, Phys. Rev. B 70 (2004) 174304.
[5] A. Funahashi, Y. Kida, K. Yanagida, T. Nohma, I. Yoneza, J. Power Sources 104 (2002) 248–252.
[6] R. Yazami, Y. Renier, B. Fultz, ECS Trans. 1 (26) (2006) 87–96.
[7] W. Lu, I. Belharounak, J. Liu, K. Amine, J. Power Sources 174 (2007) 673–677.
[8] A. Yamada, H. Koizumi, S.-I. Nishimura, N. Sonoyama, R. Kanno, M. Yonemura, T. Nakamura, Y. Kobayashi, Nat. Mater. (2006) 5.
[9] Y. Reynier, R. Yazami, B. Fultz, J. Power Sources 119–121 (2003) 850–855.
[10] Q. Wu, W. Lu, J. Prakash, J. Power Sources 88 (2000) 237–242.
[11] G. Nagasubramanian, D.H. Doughty, J. Power Sources 150 (2005) 182–186.
[12] Y.-B. He, Z.-Y. Tang, Q.-S. Song, H. Xie, Q.-H. Yang, Y.-G. Liu, G.-W. Ling, J. Power Sources 185 (2008) 526–533.
[13] J. Fan, J. Power Sources 138 (2004) 288–293.
[14] B.V. Ratnakumar, M.C. Smart, L.D. Whitcanack, R.C. Ewell, J. Power Sources 159 (2006) 1428–1439.
[15] Gremban, R., PHEV battery performance, www.calcars.org/calcars-phev-batteries18feb06-rdg.pdf 2006.
[16] A. Nourai, D. Rastler, R. Drake, T. Walker, Community Energy Storage Webinar, in Interactive Web Conference, R. Fioravanti, Editor. 2009.
[17] D. Howell, USDOE Annual Merit Review, Hydrogen Program and Vehicle Technologies Program, USDOE, Arlington, VA, 2009.
[18] D. Wang, D. Choi, J. Li, Z. Yang, Z. Nie, R. Kou, D. Hu, C. Wang, L. Saraf, J. Zhang, I. Aksay, J. Liu, ACSNano 3 (4) (2009) 907–914.
[19] Energy Information Administration, *U.S. Average Monthly Bill by Sector*. 2007. Available from: http://tonto.eia.doe.gov/ask/faq.asp.